

Trace Detection of Adulterants in Illicit Opioid Samples Using Surface-Enhanced Raman Scattering and Random Forest Classification

Published as part of *Analytical Chemistry virtual special issue* "Celebrating 50 Years of Surface Enhanced Spectroscopy".

Rebecca R. Martens, Lea Gozdziński, Ella Newman, Chris Gill, Bruce Wallace, and Dennis K. Hore*



Cite This: *Anal. Chem.* 2024, 96, 12277–12285



Read Online

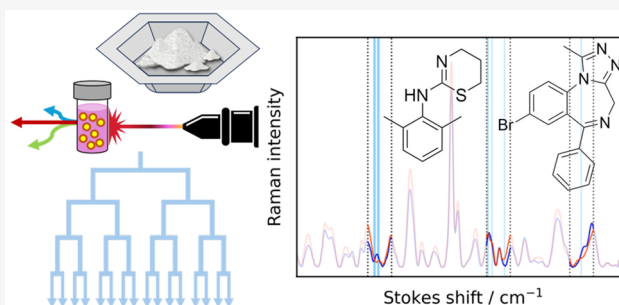
ACCESS |

Metrics & More

Article Recommendations

Supporting Information

ABSTRACT: The detection of trace adulterants in opioid samples is an important aspect of drug checking, a harm reduction measure that is required as a result of the variability and unpredictability of the illicit drug supply. While many analytical methods are suitable for such analysis, community-based approaches require techniques that are amenable to point-of-care applications with minimal sample preparation and automated analysis. We demonstrate that surface-enhanced Raman spectroscopy (SERS), combined with a random forest classifier, is able to detect the presence of two common sedatives, bromazolam (0.32–36% w/w) and xylazine (0.15–15% w/w), found in street opioid samples collected as a part of a community drug checking service. The Raman predictions, benchmarked against mass spectrometry results, exhibited high specificity (88% for bromazolam, 96% for xylazine) and sensitivity (88% for bromazolam, 92% for xylazine) for the compounds of interest. We additionally provide evidence that this exceeds the performance of a more conventional approach using infrared spectral data acquired on the same samples. This demonstrates the feasibility of SERS for point-of-care analysis of challenging multicomponent samples containing trace adulterants.



INTRODUCTION

Over the past decade, there has been a rise in deaths attributed to drug overdose, as communities across the globe struggle to understand and respond to variability in an unregulated illicit drug supply. Since the government of British Columbia, Canada declared the overdose epidemic a public health emergency in 2016, more than 13,000 people have died, making it the leading cause of unnatural death for persons aged 10–59.¹ The illicit drug market experiences a continual evolution of active components and adulterants,^{2–4} making it increasingly difficult for people who use drugs to make informed decisions and manage their dose. Synthetic opioids, specifically fentanyl and its analogues, have received a significant amount of attention since they are often the primary active in the opioid supply.^{5,6} However, there is a growing focus on detecting potent and therefore low concentration sedatives that appear as adulterants in opioid samples. Of particular importance is the presence of benzodiazepines, a broad class of depressant drugs that slow activity in the brain and nervous system.⁷ The coconsumption of benzodiazepines and opioids has been found to significantly increase the risk of respiratory depression, overdose, and death.^{1,8,9} Another recent concern is xylazine, a veterinary

tranquilizer with insufficient data on its long-term impact on humans.^{10,11} This powerful sedative has been linked to adverse effects and is increasingly found to adulterate opioid samples across British Columbia and even more pervasively in the United States and Puerto Rico.^{11–14}

Drug checking has a valuable role within responses to the overdose crisis as a harm reduction measure.^{15–17} Although the analysis methods employed range from simple antibody-based test strips^{7,18,19} to lab-based mass spectrometry,^{20,21} drug checking using analytical instruments aims to detect all components present in street samples. Techniques capable of trace analysis specifically in point-of-care settings are required. However, it remains challenging for a single instrument to exclusively meet the accessibility requirements for community drug checking,²² namely a simple, low cost, field-portable

Received: March 7, 2024

Revised: July 2, 2024

Accepted: July 5, 2024

Published: July 17, 2024



method that requires minimal operator training. Fourier transform infrared (FTIR) spectroscopy has largely met those requirements, revealing the bulk makeup of samples as well as many high concentration active components.^{23–25} However, it is widely regarded as having a limit of detection of 5% w/w for many drugs of interest,^{26,27} therefore making it unsuitable for trace detection. Portable Raman spectroscopy has also found application in drug checking,^{24,28–30} but with roughly the same limit of detection of FTIR and the additional complexity of interfering fluorescence, particularly from opioids.^{31–33} The inability to detect potentially harmful adulterants and a heavy reliance on manual interpretation present significant limitations to the widespread application of FTIR or Raman as exclusive drug-checking methods.

Surface-enhanced Raman spectroscopy (SERS) has a potential to meet this need, as the amplification of Raman signals through localized electromagnetic fields can provide access to suitably low concentrations of interest for drug analysis.^{34–37} SERS has demonstrated success for trace detection of adulterants in complex biological samples³⁸ and laboratory mixtures of opioid samples.^{39–42} Despite the promise of SERS, significant method development is required for it to reliably detect and differentiate trace adulterants in street drugs, often involving interferences in complex mixtures.^{3,43} Progress in this area has simultaneously focused on the platform itself, including optimizing the design of SERS substrate, both in general and for specific analytes,^{44–47} and the associated analysis methods.^{44,48,49} The success of manual spectral interpretation is often limited for SERS,⁵⁰ and there is a significant interest in the application of chemometric approaches.^{36,51–54} Unsupervised machine learning (ML) methods such as principal component analysis (PCA), have been demonstrated for the detection of fentanyl using SERS spectra of binary drug mixtures.⁵⁵ However, given the variability of SERS measurements, these unsupervised ML techniques often struggle to differentiate trace components as the complexity of the sample matrix increases.⁵⁶ Supervised ML techniques have more advanced decision-making abilities and are therefore useful for more complex samples with multiple components.^{57–59} Among these, random forest (RF) classification⁶⁰ employs multiple decision trees to make predictions based on characteristic features, thereby improving overall accuracy and generalization capabilities. Previous work has centered on the analysis of laboratory drug mixtures, showcasing notable success when using SERS for identifying fentanyl in heroin down to submicrogram concentrations,³⁹ and RF has proven to enhance the identification of components within increasingly complicated drug mixtures when employing traditional Raman spectroscopy techniques.⁶¹ This illustrates the synergy of combining the heightened sensitivity of SERS with the robust predictive capabilities of RF for the detection of trace adulterants within real-world samples in the illicit supply.

In this study, we employ random forest classifiers trained on FTIR and SERS spectral data from illicit drug samples acquired as a part of a community drug checking service. We focus on two common adulterants that are frequently present in opioid samples and typically in trace amounts, below the limit of detection of FTIR instruments. The first is bromazolam, a benzodiazepine⁶² that is the brominated version of alprazolam (Xanax). This is an important illustration of how SERS can be used to differentiate compounds with varying potency and pharmacological effects within the benzodiazepine class. The

second example is the detection of xylazine, a more challenging compound to identify due to strong spectral interferences. We have found the overall accuracy and specificity of the SERS method in the classification of adulterants to be superior to what can be achieved using FTIR data, when both types of spectra are analyzed using optimized RF models. This illustrates the potential of a simple and sensitive SERS technique to be successfully implemented in a point-of-care community drug checking application.

METHODS

Materials and Sample Selection. 50 nm gold nanoparticle (AuNP) solution (BBI Solutions, UK), magnesium sulfate anhydrous certified powder (MgSO₄, Fisher Chemical), and deionized water (18.2 MΩ·cm, Barnstead Nanopure water, Thermo Fisher Scientific) were used for SERS sample preparation. All drug samples used in this study were acquired from Substance, the Vancouver Island Drug Checking Project,^{25,63} as part of our ongoing drug-checking service in Victoria BC, Canada. All samples were analyzed to determine drug composition through benzodiazepine immunoassay test strips (Rapid Response, BTNX) and paper-spray mass spectrometry (TSQ Fortis, Thermo Fisher Scientific). The samples selected for this study ($n = 218$) were received in powdered form and were identified as opioid samples, with either fentanyl, fluorofentanyl, or heroin as the primary active components. In addition to the main active opioids, the samples chosen had diverse combinations of cutting agents, opioid analogues, and adulterants. The breakdown of the components identified in the selected samples is shown in Table 1.

Table 1. Compounds Identified by Paper Spray Mass Spectrometry and Benzodiazepine Immunoassay Test Strips in Training and Testing Sets

Compound	Number found	
	Training Set ($n = 168$)	Testing Set ($n = 50$)
Fentanyl	134	46
Caffeine	143	45
Fluorofentanyl	106	33
Bromazolam	65	25
Xylazine	41	25
ANPP	19	10
Chloroisobutyl Fentanyl	14	2
Benzodiazepine (Undifferentiated)	7	4
Etizolam	6	3
Flubromazepam	5	2
Heroin	4	2
Flualprazolam	4	2
Isobutyl Fentanyl	3	2
Acetylfentanyl	3	1
Acetylcodeine	2	0
Carfentanil	2	0
Metonitazene	1	0
N-Desethyl Isotonitazene	1	0
Flubromazolam	1	2
Morphine	1	0
Acetylmorphine	1	0
4-Anilino-Boc-Piperidine	0	1

Table 2. Investigation of RF Hyperparameters and Spectral Preprocessing Techniques Using a 5-Fold Cross-Validation Grid Search for (a) Bromazolam and (b) Xylazine, Showing the Combinations Tested and the Optimal Set of Parameters Selected Based on F1 Score

Parameter Name	Description	Grid Search Values	SERS		FTIR		
			Best Parameter	F1 Score	Best Parameter	F1 Score	
a. Bromazolam							
n_estimators	number of trees in RF	5, 10, 15, 20, 30, 40, 50, 100, 150, 200, 300, 400, 500, 800, 1000	800		40		
max_depth	maximum depth of a single tree	None, 1, 2, 3, 4, 5	None		5		
min_samples_leaf	minimum number of samples required to be at a leaf node	1, 2, 3, 4, 5, 10, 15, 20, 30, 40, 50	3	0.891	4	0.737	
deriv	order of derivatives of the spectral data	0, 1, 2	1		2		
norm	normalization process of the spectral data	'min-max', 'snv', 'none', 'area'	'none'		'none'		
b. Xylazine							
n_estimators	number of trees in RF	5, 10, 15, 20, 30, 40, 50, 100, 150, 200, 300, 400, 500, 800, 1000	40		5		
max_depth	maximum depth of a single tree	None, 1, 2, 3, 4, 5	3		None		
min_samples_leaf	minimum number of samples required to be at a leaf node	1, 2, 3, 4, 5, 10, 15, 20, 30, 40, 50	4	0.805	5	0.499	
deriv	order of derivatives of the spectral data	0, 1, 2	0		2		
norm	normalization process of the spectral data	'min-max', 'snv', 'none', 'area'	'snv'		'min-max'		

A subset of samples ($n = 50$) was selected as the test set for model validation using both SERS and FTIR-based platforms. Among these, $n = 25$ samples contained bromazolam (median 6.59% w/w) and $n = 25$ samples contained xylazine (median 4.35% w/w). These concentrations refer to the ratio of the target drug to the total sample weight. The specific makeup of the testing group was organized to maintain the complexity of these multicomponent opioid samples as seen in Table 1, with each sample of the $n = 50$ subset categorized into one of four groups: containing both bromazolam and xylazine ($n = 13$), only bromazolam ($n = 12$), only xylazine ($n = 12$), and those containing neither adulterant ($n = 13$).

Sample Preparation and Data Acquisition. SERS Measurements. SERS measurements were performed using a portable Raman spectrometer (Resolve, Agilent Technologies, Santa Clara, USA) equipped with an 830 nm excitation source at 100–475 mW variable power as described previously.⁴³ Approximately 1.5 mg of powdered opioid sample was added to ≈ 700 μL of deionized water. The solution was then vortexed and heated until dissolved. 70 μL of the sample solution was added to 1.42 mL of the 50 nm gold nanoparticle solution. Solutions were vortexed for 30 s and 10 μL of MgSO_4 was added as an aggregating agent. The final 1.5 mL solution was vortexed a final time for approximately 10 s. Spectra were recorded between 200–2000 cm^{-1} at a constant laser power, 2 s integration time, and 10 averages. Automated baseline, fluorescence, and cosmic ray correction procedures were applied by instrument firmware.⁶⁴

FTIR Measurements. FTIR measurements were recorded with a portable FTIR spectrometer (Agilent 4500a, Santa Clara, CA, USA) fitted with a single-bounce 45° diamond attenuated total reflectance (ATR) sampling system. The infrared (IR) spectra for the powdered opioid samples were recorded in the 650–4000 cm^{-1} region using a resolution of 4 cm^{-1} .

Mass Spectrometry Measurements. All samples used in this study were tested using a TSQ Fortis triple quadrupole mass spectrometer and a VeriSpray Paper Spray ion source (Thermo Fisher Scientific, San Jose, CA, USA). Information

regarding the method, calibration and data analysis can be found in recent publications.^{20,65–67} Briefly, 0.5–2.1 mg of the sample was dissolved into 1.2 mL of methanol and vortexed to prepare a solution in the range of 1 mg/mL. 1 μL of the solution was diluted in an internal standard solution to acquire a final concentration of 6 $\mu\text{g}/\text{mL}$. 10 μL of the spiked solution was spotted on the VeriSpray sample plate for MS analysis.

Data Processing and ML Model Development. Outlier Detection Method. The spectral data for all samples in the training set ($n = 168$) were preprocessed by first subtracting the mean and scaling to unit variance using the scikit-learn package⁶⁸ in python. Principal component analysis (PCA), was used to distinguish high variance outliers that could reduce random forest model performance. The selection of outliers was then performed using the minimum covariance determinant (MCD) method, and Mahalanobis distances were computed. Outliers were identified based on a threshold derived from a χ^2 distribution. This outlier detection method restricts the training libraries to exclusively complex multicomponent samples that share commonality within the first two principal components. The outliers detected from both the SERS and FTIR training libraries exhibited irregularities in the spectral features as compared to the other samples in PCA. These outliers corresponded to samples with high benzodiazepine concentration and unique bulk cutting agents. The data determined to be outliers were removed, and the spectra of the established training set for SERS ($n = 151$) and FTIR ($n = 153$) were used for subsequent hyperparameter tuning.

Hyperparameter Tuning for a Random Forest Binary Classifier. Binary classification for the prediction of bromazolam and xylazine in the SERS training sets was performed using a random forest classifier model (scikit-learn). The default criterion of Gini impurity was used. Optimization of the preprocessing methods (derivatives and normalization) and hyperparameters (number of decision trees, maximum depth, and minimum samples per leaf) for the RF classifier was conducted using a 5-fold cross-validation grid search. This process tested 11,880 parameter combinations for bromazolam and xylazine labeled independently. Optimal hyperparameter

values were selected based on the highest F1 scores obtained through grid search. This tuning method was also performed using the IR training set to establish IR-based RF models with the same learning metrics. Results for the optimized model parameters for SERS and IR spectral data are shown for bromazepam in Table 2a and xylazine in Table 2b.

RESULTS AND DISCUSSION

Bromazepam Detection. Model Optimization. The optimized RF binary classifiers for predicting bromazepam using SERS and IR spectral data demonstrated robust performance, yielding F1 scores of 0.891 and 0.737, respectively, during cross-validation on the training set (Table 2a). The higher F1 score of 0.891 obtained by the SERS model suggests superior precision and recall balance, indicating its effectiveness in accurately identifying positive instances within the SERS training set. Notably, the ideal parameter for optimizing SERS spectra emphasized the first-order derivative, which is particularly beneficial for improving the resolution of overlapping peaks, a common occurrence in samples with structurally similar components. This characteristic could elucidate the model's effectiveness at differentiating bromazepam features from other benzodiazepines in complex mixtures, enhancing model sensitivity to subtle spectral variations. Additionally, the large number of decision trees (800) selected for the SERS model could contribute to its high F1 score, as this helps to reduce overfitting and captures a more comprehensive representation of data patterns. The IR model, with an F1 score of 0.737, also exhibits relatively high initial predictive performance. These results underscore the capacity of the model to discern bromazepam patterns in the respective spectral data sets, with the SERS model showing a particular advantage in achieving a harmonized trade-off between precision and recall. The initial success observed in the predictive performance of the SERS model suggests that the features in SERS spectra allow for more accurate detection of bromazepam.

SERS Model Visualization. The mean spectra of bromazepam-positive and bromazepam-negative samples in the training library were used to understand the classification basis of the SERS model, as depicted in Figure 1a. The blue bands overlaid on the mean spectra represent the top 20 features extracted by the model. The wavenumber bands selected constitute the features with the highest importance degree, as calculated by the Gini index, that contribute to the identification of bromazepam by the RF model. Among the identified feature importance variables (FIVs), 14 were notably concentrated within the 650–750 cm^{-1} region. These were evenly distributed, split between the initial rise (675–681 cm^{-1}) and subsequent decline (691–696 cm^{-1}) of intensity around the distinctive band observed in the mean bromazepam-positive spectrum at 690 cm^{-1} . These features seem to correlate with the rates of change both preceding and following the band, likely a reflection of the model's selection to use the first-order derivative as the optimal spectral preprocessing parameter. This band appears to correspond to a non-obstructed spectral region and aligns with a characteristic peak visible in the SERS spectrum of a single component bromazepam street sample shown in Figure 2, largely accredited to C–Br stretching,^{69,70} unique to bromazepam that distinguishes it from other triazolobenzodiazepines. However, it is important to note that the peak highlighted by the FIVs is intended solely for illustrating the classification

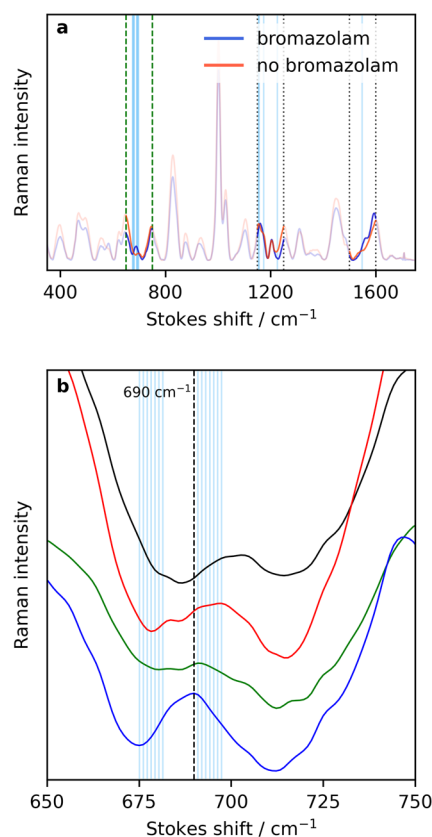


Figure 1. (a) Mean spectral data for bromazepam-positive and bromazepam-negative samples in the training set overlaid with vertical blue lines representing the top 20 features extracted by the model. Spectral regions with feature presence are highlighted. (b) Detailed view of the 650–750 cm^{-1} region with stacked mean spectra for different opioid drug combinations: opioid-only (black), adulterants other than bromazepam (red), bromazepam and additional adulterants (green), and bromazepam-only (blue).

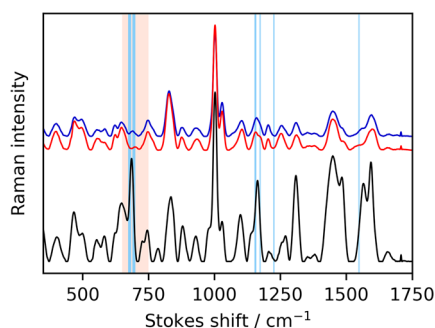


Figure 2. Mean SERS spectral data for bromazepam-positive (blue) and bromazepam-negative (red) samples in the training set compared to a single-component bromazepam street sample (black). Vertical lines represent the top 20 features extracted by the bromazepam SERS model. The characteristic spectral region of 650–750 cm^{-1} is highlighted.

framework of the SERS model and is not meant to provide information that could be used for manual interpretation of the spectra. Characterization of the band in the concentrated FIV region is further evaluated by analyzing the mean spectra of various combinations that exist within the opioid sample training set illustrated in Figure 1b. In order to ascertain whether bromazepam is the primary contributor to the band,

opioid samples adulterated exclusively with bromazepam were compared against samples containing a mixture of adulterants, samples without bromazepam adulteration, and unadulterated opioid samples. Both mean spectra for samples not containing bromazepam did not possess the characteristic band at 690 cm^{-1} , and while less pronounced, evidence of the band was still visually apparent for the mean spectrum of samples containing bromazepam and other adulterants.

Following this, a second model was developed where the spectral training data was restricted to the $650\text{--}750\text{ cm}^{-1}$ region, thereby focusing on the area with the most significant contribution to bromazepam characterization. This targeted approach aims to streamline the development of a secondary RF model (Table S1) for the detection of bromazepam in low confidence samples in the test set, as detailed in the Supporting Information.

Model Application and Performance. A receiver operating characteristic (ROC) curve was used to assess classifier accuracy and determine optimal thresholds for classification using the predicted probability scores of the SERS and IR models on the test set. These ROC curves are plotted using varying threshold values as illustrated in Figure 3.

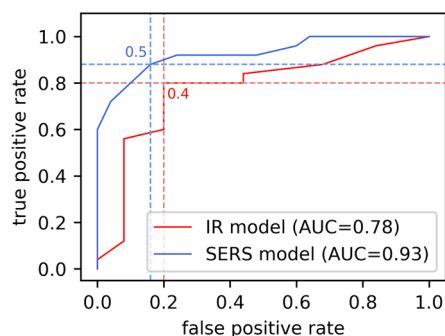


Figure 3. Comparison between the bromazepam SERS model and bromazepam IR model prediction results on the test set ($n = 50$). The ROC curves illustrate the true positive rate and false positive rate across various classification thresholds for bromazepam detection. Optimal threshold selection for balancing sensitivity and specificity and area under the curve (AUC) is highlighted for both models.

The area under the curve (AUC) was used to evaluate the performance of the binary classification models across the chosen range of thresholds. AUC values of 0.93 and 0.78 were determined for the SERS and IR models, respectively, indicating good discriminatory power. However, the high AUC value of 0.93 demonstrates the increased capability of SERS model in distinguishing true bromazepam from false bromazepam, irrespective of the classification threshold.

Optimal thresholds for the SERS (0.5) and IR (0.4) models were identified by balancing sensitivity and specificity using Youden's J statistic. Test set prediction results for bromazepam were generated using the corresponding threshold values. A low confidence range (LCR) between 0.5 and 0.6 was established for the SERS model based on the minimum and maximum probability scores derived from false positive samples in the test set. Subsequently, all samples with scores in the LCR ($n = 11$) were subject to additional testing using the targeted secondary bromazepam SERS model (Figures S1–S2) trained on restricted spectral regions as detailed in the Supporting Information. The LCR prediction results were then reintegrated with the test set for model evaluation.

The SERS and IR models prediction results of the test set used for model evaluation are illustrated in Table 3.

Table 3. Bromazepam Prediction Results for Samples in the Test Sets ($n = 50$) for SERS and IR Models

Result	IR Model	SERS Model
true positive	20	22
true negative	20	22
false positive	5	3
false negative	5	3

Given the complexity of opioid samples and the impact of misidentifying powerful sedatives in the sample, the ability to detect bromazepam with high sensitivity is of greater importance than specificity. While both remain integral to assessing the performance of the model, increasing the number of true positives and lowering the number of false negatives is a significant factor in the context of this work. Both the SERS and IR models demonstrated high predictive success in the positive and negative class, showing balanced sensitivity and specificity (Table 4a). The IR model correctly identified 12 out of the 17 bromazepam-positive samples below its widely accepted threshold of 5% w/w.^{26,27,31} The expanded limit of detection (LOD) and the relatively high accuracy of the IR model (80%) is likely a consequence of the distinct peaks of bromazepam in the $750\text{--}850\text{ cm}^{-1}$ region (Figure S3). In comparison, the SERS model correctly identified 15 out of 17 samples with bromazepam concentrations of <5% w/w, with the lowest detected concentration being 0.32% w/w, the highest at 36% w/w. This level of performance illustrates the compatibility of the RF-based approach with both SERS and IR spectral data in trace detection of bromazepam.

Xylazine Detection. Model Optimization. The optimized RF binary classifiers for predicting xylazine using the SERS and IR spectral data demonstrated varied performance, yielding F1 scores of 0.805 and 0.499, respectively, during cross-validation (Table 2b). The resulting SERS model F1 score of 0.805 indicates a high precision and recall within the training set and notably prioritized normalization over derivative-based parameters for optimizing spectra. The standard normal variate (SNV) normalization selected for the model is a useful technique in reducing SERS intensity variations and in standardizing the scale of spectral features. The IR model demonstrated weak initial predictive performance, as evidenced by an F1 score of 0.499 and a particularly low mean sensitivity (recall) of 0.439, averaged across the five validation folds. The selection of 5 decision trees suggests the IR model has low complexity for the intricacies of the sample matrices it is analyzing and may be making simplistic assumptions of patterns regarding xylazine to improve its performance. The selection of min-max normalization is indicative of a high degree of spectral overlap, with more dominating components in the mixture presenting a challenge for the classification of xylazine using the IR method.

SERS Model Visualization. Mean xylazine-positive and xylazine-negative SERS spectra of samples in the training set and the top 20 features extracted by the model are illustrated in Figure 4a. The distinct peak observed at 1490 cm^{-1} in the mean xylazine-positive spectrum, accompanied by a nearby feature importance band at 1495 cm^{-1} (Figure 4a), was also detected in benzodiazepine-only mixtures (Figure S4). This spectral region is closely associated with aromatic ring C–C

Table 4. Summary of Accuracy, Precision, Sensitivity, Specificity, Positive Predictive Value (PPV), and Negative Predictive Value (NPV) for Opioid Samples ($n = 50$) Tested with RF Models: Model Prediction Results for IR and SERS Data for (a) Bromazolam and (b) Xylazine Detection

Model	Accuracy (%)	Precision (%)	Sensitivity (%)	Specificity (%)	PPV (%)	NPV (%)
a. Bromazolam						
IR	80	80	80	80	80	80
SERS	88	88	88	88	88	88
b. Xylazine						
IR	68	62	96	40	62	91
SERS	94	96	92	96	96	92

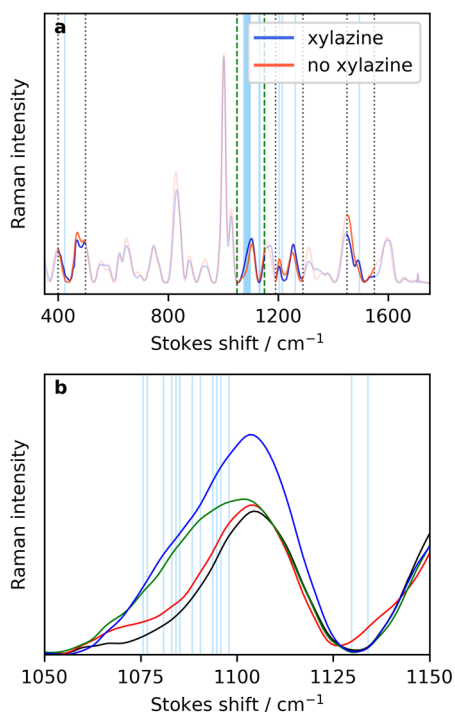


Figure 4. (a) Mean spectral data for xylazine-positive and xylazine-negative samples in the training set overlaid with vertical blue lines representing the top 20 features extracted by the model. (b) Detailed view of the 1050–1150 cm^{-1} region with overlaid mean spectra for different opioid drug combinations: opioid-only (black), adulterants other than xylazine (red), xylazine and additional adulterants (green), and xylazine-only (blue).

stretching vibrations and N–C vibrations, which are common in most benzodiazepines.^{71–74} Specifically, etizolam exhibits a characteristic peak at 1491 cm^{-1} ,⁴³ and other triazolobenzodiazepines show significant band presence in the 1400–1500 cm^{-1} range,⁷¹ which are frequent adulterants found in the SERS training group. Therefore, the shoulder band at 1490 cm^{-1} , experiencing significant overlap within the matrix, was determined to lack specificity for xylazine characterization and was consequently disregarded in the development of the secondary model. However, Many of the FIVs accumulate in the 1050–1150 cm^{-1} region and 14 are particularly clustered around the 1075–1098 cm^{-1} band edge. Although this region also contains contributions from additional components in the sample matrix, there is evidence of broadening due to the presence of xylazine. The FIVs and increased intensity firmly align with the strong xylazine peak visible in the single component SERS spectrum seen in Figure 5. The mean spectra of different combinations of opioid samples in the training set,

as shown in Figure 4b, further illustrate the intensity variations of the peak.

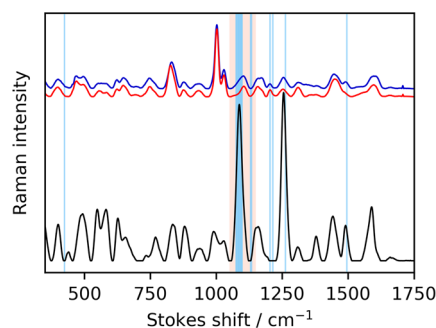


Figure 5. Mean SERS spectral data for xylazine-positive (blue) and xylazine-negative (red) samples in the training set compared to a single-component xylazine street sample (black). Vertical lines represent the top 20 features extracted by the xylazine SERS model. The characteristic spectral region of 1050–1150 cm^{-1} is highlighted.

Following this, the spectral training data was restricted exclusively to the xylazine characteristic SERS region of 1050–1150 cm^{-1} and used for the development of a secondary RF model (Table S1) targeted at low confidence samples in the test set, as detailed in the Supporting Information.

Model Application and Performance. ROC analysis was performed on the SERS and IR models for the test set as shown in Figure 6.

AUC values of 0.94 and 0.72 were calculated for the SERS and IR models, respectively. The SERS model reflects high discriminatory power across the range of thresholds,

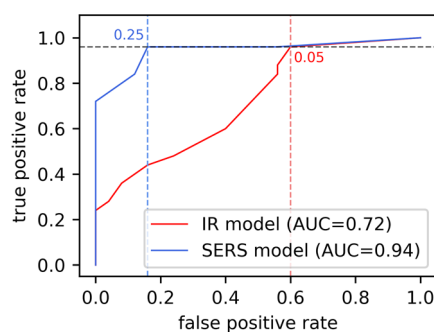


Figure 6. Comparison between the xylazine SERS model and xylazine IR model prediction results of xylazine on the test set ($n = 50$). The ROC curves illustrate the true positive rate and false positive rate across various classification thresholds for xylazine detection. Optimal threshold selection for balancing sensitivity and specificity and area under the curve (AUC) is highlighted for both models.

illustrating the utility of SERS for the accurate detection of xylazine with little influence from competing spectral components in the sample matrix. The IR model demonstrated poor performance across the range of predicted probabilities, with prediction results approaching that of a baseline classifier.

Optimal predicted probability score thresholds for the SERS (0.25) and IR (0.05) models were calculated and applied to the test set. The LCR for the SERS model was established to be between 0.25 and 0.45 and all samples with scores in the LCR ($n = 10$) underwent additional testing using the targeted secondary xylazine SERS model (Figures S1–S2) detailed in Supporting Information. The LCR prediction results were then reintegrated with the test set for model evaluation.

Xylazine prediction results are shown in Table 5 and were used to evaluate the performance of the SERS and IR models.

Table 5. Xylazine Prediction Results of the Test Set ($n = 50$) for the SERS and IR models

Result	IR Model	SERS Model
true positive	24	23
true negative	10	24
false positive	15	1
false negative	1	2

The SERS model correctly identified 23 out of the 25 xylazine-positive samples and 24 out of the 25 xylazine-negative samples. Two positive trace concentration samples (both below 1% w/w) were misidentified, yet the model successfully distinguished all other samples in the test set containing xylazine (0.15–15% w/w), demonstrating a robust prediction range.

The results of the SERS and IR models shown in Table 4b coincide with the performance predictions of their respective F1 scores (0.801 and 0.499) and AUC values (0.94 and 0.72). The SERS model exhibited the ability to distinguish true negatives from true positives while minimizing false negatives and false positives (94% accuracy and 96% precision). By comparison, the IR model correctly identified 24 out of 25 true positive samples and incorrectly claimed 15 false positives, indicating superior sensitivity but lacking discriminatory power. This tendency to overpredict resulted in lower accuracy (68%) and precision (62%) for the IR model (Table 4b). Over prediction of the positive class could be attributed to underfitting during model training, further aggravated by a low prediction threshold of 0.05 that hampers performance for negative instances. The suboptimal performance of the IR model may be indicative of significant spectral obstruction, particularly in the 1600–1650 cm^{-1} region where xylazine's characteristic features⁷⁵ experience strong interference from the vibrational bands of opioids and common cutting agents.⁷⁶ Further evidence appears in the features selected for the xylazine IR model that do not correspond to the strong characteristic peaks in the single component xylazine reference spectrum, and the lack of distinguishable peaks in the xylazine-positive mean spectrum (Figure S5). This points to the limitations of IR for detecting low concentrations of xylazine in complex opioid mixtures, both in the case of manual interpretation and model development.

Consequence for Drug Checking. The implementation of a simple random forest classification method provides a valuable tool for standardizing spectral analysis in point-of-care services. However, despite the improved LOD of bromazepam

afforded by the IR model, the poor xylazine performance underscores the limitations of techniques based on IR absorption in detecting low concentration adulterants. The detection of both bromazepam and xylazine was highly improved with the use of RF classification coupled with SERS. The accurate differentiation of two common adulterants in concentrations less than 1% w/w using the SERS based models illustrates the superior sensitivity that can be achieved without sacrificing the benefits of affordable and accessible technology desired by drug checkers. The application of a straightforward and uniform SERS sample preparation method enables facile integration into drug checking training protocols. The success of these models in identifying bromazepam and xylazine using SERS data may be attributed to the fact that the training set was established using drugs collected from a community harm reduction service. Street samples of illicit opioids have inherent complexities that are often a significant challenge to accurately replicate for model development using laboratory standards or simulated data. This work showcases the predictive enhancements of binary classifiers particularly when the learning metrics of models reflect what they analyze, warranting the continued exploration of tailoring models to real-world illicit samples. It should be noted that the unpredictable nature of illicit street samples can also introduce complications in model development. The variability of compounds and adulterant concentrations in street samples, limits its use in the development of quantitative models. The complex nature of these samples also means the model performance may be influenced by variations in matrix components not encountered in the training phase. Future SERS studies alongside targeted mass spectrometry to develop larger labeled data sets could vastly benefit the drug checking community and expand automated algorithms for the rapid and accurate detection of trace adulterants in complex mixtures.

CONCLUSIONS

We have demonstrated the trace detection of two common adulterants, bromazepam and xylazine, in complex illicit opioid samples using a random forest classifier trained on SERS spectral data. In both cases, the performance exceeded that obtained using FTIR spectroscopy which is more commonly employed in point-of-care drug checking applications, even when similar machine learning approaches were used. Visualization of the features determined to have the highest contribution to the predictive success revealed characteristic regions within the SERS spectra of bromazepam and xylazine. This enabled a secondary model to be trained that further improved sensitivity and specificity in the classification of samples in the low confidence range. Overall, this illustrates the capability of SERS when applied to real-world drug samples for the accurate detection and differentiation of potentially harmful sedatives that are increasingly present in the opioid supply.

ASSOCIATED CONTENT

Supporting Information

The Supporting Information is available free of charge at <https://pubs.acs.org/doi/10.1021/acs.analchem.4c01271>.

Information on the composition of samples in the training and test sets; additional spectra; targeted secondary model development (PDF)

AUTHOR INFORMATION

Corresponding Author

Dennis K. Hore – Department of Chemistry, University of Victoria, Victoria, British Columbia V8W 3V6, Canada; Department of Computer Science, University of Victoria, Victoria, British Columbia V8W 3P6, Canada; Canadian Institute for Substance Use Research, University of Victoria, Victoria, British Columbia V8W 2Y2, Canada; orcid.org/0000-0001-8969-9644; Email: dkhore@uvic.ca

Authors

Rebecca R. Martens – Department of Chemistry, University of Victoria, Victoria, British Columbia V8W 3V6, Canada

Lea Gozdziński – Department of Chemistry, University of Victoria, Victoria, British Columbia V8W 3V6, Canada

Ella Newman – Department of Chemistry, University of Victoria, Victoria, British Columbia V8W 3V6, Canada

Chris Gill – Department of Chemistry, Vancouver Island University, Nanaimo, British Columbia V9R 5S5, Canada; Department of Chemistry, University of Victoria, Victoria, British Columbia V8W 3V6, Canada; Department of Environmental and Occupational Health Sciences, University of Washington, Seattle, Washington 98195, United States; Canadian Institute for Substance Use Research, University of Victoria, Victoria, British Columbia V8W 2Y2, Canada; orcid.org/0000-0001-7696-5894

Bruce Wallace – School of Social Work and Canadian Institute for Substance Use Research, University of Victoria, Victoria, British Columbia V8W 2Y2, Canada

Complete contact information is available at:

<https://pubs.acs.org/10.1021/acs.analchem.4c01271>

Notes

The authors declare no competing financial interest.

ACKNOWLEDGMENTS

This project was funded by a grant from the Health Canada Substance Use and Addictions program (1819-HQ-000042), with additional support from the Vancouver Foundation (F0120-5607), BC Ministry of Mental Health & Addictions, and Vancouver Island Health Authority. High performance computing support and server resource allocation was provided by the University of Victoria and the Digital Research Alliance of Canada. Allie Miskulin provided support for the PS-MS data acquisition.

REFERENCES

- (1) BC Coroners Service. *Illicit Drug Toxicity Deaths in BC*, 2023. <https://www2.gov.bc.ca/gov/content/life-events/death/coroners-service/statistical-reports>.
- (2) Larnder, A.; Saatchi, A.; Borden, S. A.; Moa, B.; Gill, C. G.; Wallace, B.; Hore, D. *Drug Alcohol Depend* **2022**, *235*, 109427.
- (3) Bhuiyan, I.; Tobias, S.; Ti, L. *Am. J. Drug Alcohol Abuse* **2023**, *49*, 685–690.
- (4) Beaulac, M.; Richardson, L.; Tobias, S.; Lysyshyn, M.; Grant, C.; Ti, L. *Int. J. Drug Policy* **2022**, *105*, 103707.
- (5) Misailidi, N.; Papoutsis, I.; Nikolaou, P.; Dona, A.; Spiliopoulou, C.; Athanasiadis, S. *Forensic Toxicol.* **2018**, *36*, 12–32.
- (6) Borden, S.; Mercer, S. R.; Saatchi, A.; Wong, E.; Stefan, C. M.; Wiebe, H.; Hore, D. K.; Wallace, B.; Gill, C. G. *Drug Test Anal* **2023**, *15*, 484–494.
- (7) Laing, M. K.; Ti, L.; Marmel, A.; Tobias, S.; Shapiro, A. M.; Laing, R.; Lysyshyn, M.; Socias, M. E. *Int. J. Drug Policy* **2021**, *93*, 103169.

- (8) Russell, C.; Law, J.; Bonn, M.; Rehm, J.; Ali, F. *Int. J. Drug Policy* **2023**, *111*, 103933.
- (9) Johnson, C. F.; Barnsdale, L. R.; McAuley, A. *Investigating the Role of Benzodiazepines in Drug-Related Mortality – A Systematic Review Undertaken on Behalf of The Scottish National Forum on Drug-Related Deaths*; NHS Health Scotland: Edinburgh, 2016.
- (10) Sue, K. L.; Hawk, K. *Addiction* **2024**, *119*, 606–608.
- (11) Kacinko, S. L.; Mohr, A. L. A.; Logan, B. K.; Barbieri, E. J. *J. Anal. Toxicol.* **2022**, *46*, 911–917.
- (12) Tobias, S.; Shapiro, A. M.; Wu, H.; Ti, L. *Can. J. Addiction* **2020**, *11*, 28–32.
- (13) Bowles, J. M.; McDonald, K.; Maghsoudi, N.; Thompson, H.; Stefan, C.; Berialt, D. R.; Delaney, S.; Wong, E.; Werb, D. *Harm Reduct. J.* **2021**, *18*, 104.
- (14) Torruella, R. A. *Subst. Abuse Treat. Prev. Policy* **2011**, *6*, 7.
- (15) Measham, F. *Br. J. Clin. Pharmacol.* **2020**, *86*, 420–428.
- (16) Laing, M. K.; Tupper, K. W.; Fairbairn, N. *Int. J. Drug Policy* **2018**, *62*, 59–66.
- (17) Wallace, B.; van Roode, T.; Burek, P.; Pauly, B.; Hore, D. *Drugs Education Prevention Policy* **2023**, *30*, 443–452.
- (18) Shapiro, A.; Sim, D.; Wu, H.; Mogg, M.; Tobias, S.; Patel, P.; Ti, L. *Detection of Etizolam, Flualprazolam, and Flubromazolam by Benzodiazepine-Specific Lateral Flow Immunoassay Test Strips*; British Columbia Centre on Substance Use, July 2020.
- (19) Green, T. C.; Park, J. N.; Gilbert, M.; McKenzie, M.; Struth, E.; Lucas, R.; Clarke, W.; Sherman, S. G. *Int. J. Drug Policy* **2020**, *77*, 102661.
- (20) Gozdziński, L.; Aasen, J.; Larnder, A.; Ramsay, M.; Borden, S. A.; Saatchi, A.; Gill, C. G.; Wallace, B.; Hore, D. K. *Int. J. Drug Policy* **2021**, *97*, 103409.
- (21) Vandergrift, G. W.; Gill, C. G. *J. Mass Spectrom.* **2019**, *54*, 729–737.
- (22) Thompson, H.; McDonald, K. *Int. J. Environ. Res. Public Health* **2023**, *20*, 6486.
- (23) Gozdziński, L.; Hutchison, A.; Wallace, B.; Gill, C.; Hore, D. *Drug Test Anal.* **2024**, *16*, 83–92.
- (24) Gozdziński, L.; Wallace, B.; Hore, D. *Harm Reduction J.* **2023**, *20*, 39.
- (25) Wallace, B.; Hills, R.; Rothwell, J.; Kumar, D.; Garber, I.; van Roode, T.; Larnder, A.; Pagan, F.; Aasen, J.; Weatherston, J.; Gozdziński, L.; Ramsay, M.; Burek, P.; Azam, M. S.; Pauly, B.; Storey, M.-A.; Hore, D. K. *Drug Test Anal.* **2021**, *13*, 734–746.
- (26) Bunaciu, A. A.; Aboul-Enein, H. Y.; Fleschin, S. *Appl. Spectrosc. Rev.* **2010**, *45*, 206–219.
- (27) Tobias, S.; Shapiro, A. M.; Grant, C. J.; Patel, P.; Lysyshyn, M.; Ti, L. *Drug Alcohol Depend* **2021**, *218*, 108300.
- (28) Gozdziński, L.; Ramsay, M.; Larnder, A.; Wallace, B.; Hore, D. K. *J. Raman Spectrosc.* **2021**, *52*, 1308–1316.
- (29) Gerace, E.; Seganti, F.; Luciano, C.; Lombardo, T.; Di Corcia, D.; Teifel, H.; Vincenti, M.; Salomone, A. *Drug Alcohol Rev.* **2019**, *38*, 50–56.
- (30) Mullin, A.; Scott, M.; Vaccaro, G.; Gittins, R.; Ferla, S.; Schifano, F.; Guirguis, A. *Int. J. Environ. Res. Public Health* **2023**, *20*, 4793.
- (31) Johnson, C. S.; Stansfield, C. R.; Hassan, V. R. *Forensic Sci. Int.* **2020**, *313*, 110367.
- (32) Vankeirsbilck, T.; Vercauteren, A.; Baeyens, W.; Van der Weken, G.; Verpoort, F.; Vergote, G.; Remon, J. P. *Trends Anal. Chem.* **2002**, *21*, 869–877.
- (33) Lanzarotta, A.; Witkowski, M.; Batson, J. J. *Forensic Sci.* **2020**, *65*, 421–427.
- (34) Mabbott, S.; Alharbi, O.; Groves, K.; Goodacre, R. *Analyst* **2015**, *140*, 4399–4406.
- (35) Burr, D. S.; Fatigante, W. L.; Lartey, J. A.; Jang, W.; Stelmack, A. R.; McClurg, N. W.; Standard, J. M.; Wieland, J. R.; Kim, J.-H.; Mulligan, C. C.; Driskell, J. D. *Anal. Chem.* **2020**, *92*, 6676–6683.
- (36) Sha, X.; Fang, G.; Cao, G.; Li, S.; Hasi, W.; Han, S. *Analyst* **2022**, *147*, 5785–5795.

- (37) Segawa, H.; Fukuoka, T.; Itoh, T.; Imai, Y.; Iwata, Y. T.; Yamamuro, T.; Kuwayama, K.; Tsujikawa, K.; Kanamori, T.; Inoue, H. *Analyst* **2019**, *144*, 2158–2165.
- (38) Shende, C.; Brouillette, C.; Farquharson, S. *Analyst* **2019**, *144*, 5449–5454.
- (39) Haddad, A.; Comanescu, M. A.; Green, O.; Kubic, T. A.; Lombardi, J. R. *Anal. Chem.* **2018**, *90*, 12678–12685.
- (40) Wang, H.; Xue, Z.; Wu, Y.; Gilmore, J.; Wang, L.; Fabris, L. *Anal. Chem.* **2021**, *93*, 9373–9382.
- (41) Kimani, M. M.; Lanzarotta, A.; Batson, J. S. *J. Forensic Sci.* **2021**, *66*, 491–504.
- (42) Leonard, J.; Haddad, A.; Green, O.; Birke, R. L.; Kubic, T.; Kocak, A.; Lombardi, J. R. *J. Raman Spectrosc.* **2017**, *48*, 1323–1329.
- (43) Gozdziński, L.; Rowley, A.; Borden, S.; Saatchi, A.; Gill, C. G.; Wallace, B.; Hore, D. K. *Int. J. Drug Policy* **2022**, *102*, 103611.
- (44) Pilot, R.; Signorini, R.; Durante, C.; Orian, L.; Bhamidipati, M.; Fabris, L. *Biosensors* **2019**, *9*, 57.
- (45) Yaffe, N. R.; Ingram, A.; Graham, D.; Blanch, E. W. *J. Raman Spectrosc.* **2010**, *41*, 618–623.
- (46) Karawdeniya, B. I.; Bandara, Y. M. N. D. Y.; Whelan, J. C.; Dwyer, J. R. *ACS Appl. Nano Mater.* **2018**, *1*, 960–968.
- (47) Han, Y.; Wu, S.-R.; Tian, X.-D.; Zhang, Y. *ACS Appl. Mater. Interfaces* **2020**, *12*, 28965–28974.
- (48) Brulé, T.; Bouhelier, A.; Dereux, A.; Finot, E. *ACS Sens.* **2016**, *1*, 676–680.
- (49) Pavan Kumar, G. V.; Ashok Reddy, B. A.; Arif, M.; Kundu, T. K.; Narayana, C. J. *Phys. Chem. B* **2006**, *110*, 16787–16792.
- (50) Lai, H.; Yu, Z.; Li, G.; Zhang, Z. *J. Chromatogr. A* **2022**, *1675*, 463181.
- (51) Hu, W.; Ye, S.; Zhang, Y.; Li, T.; Zhang, G.; Luo, Y.; Mukamel, S.; Jiang, J. *J. Phys. Chem. Lett.* **2019**, *10*, 6026–6031.
- (52) Lee, S.; Oh, J.; Lee, K.; Cho, M.; Paulson, B.; Kim, J. K. *Anal. Chem.* **2022**, *94*, 17477–17484.
- (53) Luo, S.-H.; Wang, W.-L.; Zhou, Z.-F.; Xie, Y.; Ren, B.; Liu, G.-K.; Tian, Z.-Q. *Anal. Chem.* **2022**, *94*, 10151–10158.
- (54) Mirsafavi, R.; Moskovits, M.; Meinhart, C. *Analyst* **2020**, *145*, 3440–3446.
- (55) Wang, L.; Vendrell-Dones, M. O.; Deriu, C.; Dogruer, S.; de B. Harrington, P.; McCord, B. *Appl. Spectrosc.* **2021**, *75*, 1225–1236.
- (56) dos Santos, D. P.; Sena, M. M.; Almeida, M. R.; Mazali, I. O.; Olivieri, A. C.; Villa, J. E. L. *Anal. Bioanal. Chem.* **2023**, *415*, 3945–3966.
- (57) Guo, M.; Li, M.; Fu, H.; Zhang, Y.; Chen, T.; Tang, H.; Zhang, T.; Li, H. *Spectrochim. Acta, Part A* **2023**, *287*, 122057.
- (58) Seifert, S. *Sci. Rep.* **2020**, *10*, 5436.
- (59) Weng, S.; Qiu, M.; Dong, R.; Wang, F.; Huang, L.; Zhang, D.; Zhao, J. *Spectrochim. Acta, Part A* **2018**, *200*, 20–25.
- (60) Breiman, L. *Mach. Learn.* **2001**, *45*, 5–32.
- (61) Cooman, T.; Trejos, T.; Romero, A.; Arroyo, L. *Chem. Phys. Lett.* **2022**, *787*, 139283.
- (62) Edinoff, A. N.; Nix, C. A.; Odisho, A. S.; Babin, C. P.; Derouen, A. G.; Lutfallah, S. C.; Cornett, E. M.; Murnane, K. S.; Kaye, A. M.; Kaye, A. D. *Neurol. Int.* **2022**, *14*, 648–663.
- (63) Wallace, B.; Gozdziński, L.; Qbaich, A.; Shafiul, A.; Burek, P.; Hutchison, A.; Teal, T.; Louw, R.; Kielty, C.; Robinson, D.; Moa, B.; Storey, M.-A.; Gill, C.; Hore, D. *Drugs Habits and Social Policy* **2022**, *23*, 220–231.
- (64) Smith, M.; Logan, M.; Bazley, M.; Blanchfield, J.; Stokes, R.; Blanco, A.; McGee, R. *J. Forensic Sci.* **2021**, *66*, 505–519.
- (65) Miskulin, A.; Wallace, B.; Gill, C.; Hore, D. *Drug Test. Anal.* **2023**, DOI: 10.1002/dta.3630.
- (66) Borden, S. A.; Saatchi, A.; Vandergrift, G. W.; Palaty, J.; Lysyshyn, M.; Gill, C. G. *Drug Alcohol Rev.* **2022**, *41*, 410–418.
- (67) Borden, S. A.; Saatchi, A.; Krogh, E. T.; Gill, C. G. *Anal. Sci. Adv.* **2020**, *1*, 97–108.
- (68) Pedregosa, F.; Varoquaux, G.; Gramfort, A.; Michel, V.; Thirion, B.; Grisel, O.; Blondel, M.; Prettenhofer, P.; Weiss, R.; Dubourg, V.; Vanderplas, J.; Passos, A.; Cournapeau, D.; Brucher, M.; Perrot, M.; Duchesnay, E. *J. Mach. Learn. Res.* **2011**, *12*, 2825–2830.
- (69) Harkins, W. D.; Bowers, H. E. *Phys. Rev.* **1931**, *38*, 1845–1857.
- (70) Cleaver, K. D.; Davies, J. E. D.; Wood, W. J. *J. Mol. Struct.* **1975**, *25*, 222–224.
- (71) Kimani, M. M.; Smith, S. W.; Lanzarotta, A.; Brueggemeyer, J. L.; Batson, J. S. *Forensic Sci. Int.* **2022**, *338*, 111390.
- (72) Doctor, E. L. *Development of a Surface-Enhanced Raman Spectroscopy Method for the Detection of Benzodiazepines in Urine*. Ph.D. thesis, Florida International University, Miami, FL, 2014.
- (73) Neville, G. A.; Shurvell, H. F. *J. Raman Spectrosc.* **1990**, *21*, 9–19.
- (74) Neville, G. A.; Beckstead, H. D.; Shurvell, H. F. *Vib. Spectrosc.* **1991**, *1*, 287–297.
- (75) Anban, J. D.; James, C.; Kumar, J. S.; Pradhan, S. *SN Appl. Sci.* **2020**, *2*, 1685.
- (76) Ramsay, M.; Gozdziński, L.; Larnder, A.; Wallace, B.; Hore, D. K. *Vib. Spectrosc.* **2021**, *114*, 103243.